Journal of Photochemistry and Photobiology B: Biology 141 (2014) 275–282

Contents lists available at ScienceDirect

Journal of Photochemistry and Photobiology B: Biology

journal homepage: www.elsevier.com/locate/jphotobiol

Effect of dye localization and self-interactions on the photosensitized generation of singlet oxygen by rose bengal bound to bovine serum albumin

María Beatriz Espeche Turbay [a], Valentina Rey [a], Natalia M. Argañaraz [a], Faustino E. Morán Vieyra [a], Alexis Aspée [b], Eduardo A. Lissi [b], Claudio D. Borsarelli [a,*]

[a] Laboratorio de Cinética y Fotoquímica, CITSE-CONICET, Universidad Nacional de Santiago del Estero, RN9, km 1125, CP4206 Santiago del Estero, Argentina
[b] Departamento de Ciencias del Ambiente, Facultad de Química y Biología, Universidad de Santiago de Chile, USACH, Av. Bernardo O'Higgins, 3363 Santiago, Chile

ARTICLE INFO

Article history:
Received 26 July 2014
Received in revised form 20 September 2014
Accepted 23 September 2014
Available online 5 October 2014

ABSTRACT

The spectroscopic and photophysical properties of rose bengal (RB) encased in bovine serum albumin (BSA) have been examined to evaluate the photosensitized generation of singlet molecular oxygen ($^1O_2$). The results show that RB photophysical and photosensitizing properties are highly modulated by the average number of dye molecules per protein (n). At $n \ll 1$, the dye molecule is tightly located into the hydrophobic nanocavity site I of the BSA molecule with a binding constant $K_b = 0.15 \pm 0.01\ \mu M^{-1}$. The interaction with surrounding amino acids induces heterogeneous decay of both singlet and triplet excited states of RB and partially reduce its triplet quantum yield as compared with that in buffer solution. However, despite of the diffusive barrier imposed by the protein nanocavity to $^3O_2$, the quenching of $^3RB^*$:BSA generates $^1O_2$ with quantum yield $\Phi_\Delta = 0.35 \pm 0.05$. In turns, the intraprotein generated $^1O_2$ is able to diffuse through the bulk solution, where is dynamically quenched by BSA itself with an overall quenching rate constant of $7.3 \times 10^8\ M^{-1}\ s^{-1}$. However, at $n > 1$, nonspecific binding of up to ≈6 RB molecules per BSA is produced, allowing efficient static quenching of excited states of RB preventing photosensitization of $^1O_2$. These results provide useful information for development of dye-protein adducts suitable for using as potential intracellular photosensitizers.

1. Introduction

Photosensitized generation of singlet molecular oxygen ($^1O_2$) has very relevant implications in photochemistry and photobiology with several uses in different fields, such as wastewater treatment, fine chemical synthesis, and photodynamic therapy (PDT) [1–3]. In the latter case, current increasing interest is focused in the development of efficient hybrid photosensitizer systems composed by a sensitizer molecule encased either in biocompatible self-assembled structures or in biomolecules [4–6]. Recently, with the design and development of genetically-encodable fluorescent proteins, such as green fluorescent protein (GFP) family, it has been shown that they were also able to photogenerate $^1O_2$, with potential use in antimicrobial PDT applications [7]. However, most of the GFP variants showed very low quantum yield of $^1O_2$ generation, *e.g.* $\Phi_\Delta < 0.004$, because of the intrinsic low efficiency of the GFP chromophore [8]. On the contrary, it has been formerly reported that blue-light excitation of a genetically encoded flavoprotein bearing flavin mononucleotide FMN produced $^1O_2$ with quantum yield value similar to that for the free flavin ($\Phi_\Delta \approx 0.5$), giving reason to name this flavoprotein as mini-Singlet-Oxygen-Generator (miniSOG) [9]. However, later photophysical characterization studies of miniSOG demonstrated that the photosensitized efficiency of $^1O_2$ is much lower, e.g. $\Phi_\Delta \approx 0.03$, due to the role of the peptide backbone to enhance electron-transfer (Type I) in detriment of energy-transfer (Type II) mechanism [10,11].

On the other hand, as a different strategy to obtain efficient biocompatible $^1O_2$-photosensitizer systems, we have characterized the photophysical and photochemical properties of well-known Type II artificial sensitizers such as zinc phthalocyanine (ZnPc) [6], rose bengal (RB) [12], and methylene blue (MB) [13], non-covalently bound to both bovine and human serum albumins (BSA and HSA), considering the large concentration of these proteins in blood and their function in the transport and delivery of small drugs and bioactive molecules [14]. However, despite of the moderate efficiency of generation of $^1O_2$ of these supramolecular photosensitizer assemblies, the photophysical and photosensitizing properties of the dye-albumin adducts were mainly dependent on the type of binding-site in the albumin, molecular oxygen

* Corresponding author. Tel.: +54 385 4509528.
E-mail address: cdborsarelli@gmail.com (C.D. Borsarelli).

http://dx.doi.org/10.1016/j.jphotobiol.2014.09.014
1011-1344/

accessibility to the dye binding location, and also of the average number of sensitizer molecules per protein (n), being each adduct system practically a particular case of study. Therefore, the results indicate that the photoinduced generation of $^1O_2$ by sensitizers encased in proteins cavities is a rather complex issue, where all or some of the above mentioned factors can induce different effects depending on the nature of the guest sensitizer and the host protein.

For a deeper understanding of the role of these different effects on the photosensitizing properties of sensitizer-protein adducts, in this work we studied the system formed by rose bengal (RB) encased in bovine serum albumin (BSA), under concentration conditions where the protein/dye molar ratio was varied more than two-order of magnitude to analyze separately the contribution of the self-interaction and compartmentalization processes of the bound dye. The xanthene dye RB was chosen as suitable sensitizer because besides of its large quantum yield of generation of $^1O_2$ in aqueous media ($\Phi_\Delta = 0.76$) [15], their absorption and emission spectra are very sensitive to both specific and global environmental effects [15–18]. The results reported here expand those observed in our previous study of the system RB-HSA [12], demonstrating how both photophysical and photosensitizing properties of the dye-protein adduct are modulated by n, as consequence of dye self-interaction and compartmentalization effects. All together, the present results provide useful information on the role of supramolecular interactions between the dye and the albumin and also about the fate of $^1O_2$ in this type of systems, which can be applied for the further development of non-covalent sensitizer-protein adducts with suitable efficiency of $^1O_2$ generation.

2. Experimental section

2.1. Materials

Rose bengal (RB), chemically 4,5,6,7-tetrachloro 2′,4′,5′,7′-tetraiodo-fluorescein di sodium salt, bovine serum albumin (BSA, ⩾98% free lipids), Trizma® base (tris[hydroxymethyl]-aminomethane, electrophoresis reagent minimum 99.9%) and deuterium oxide and chloride, 99.9 atom %D, were purchased from Sigma–Aldrich Argentina (Buenos Aires, Argentina). Hydrochloric acid (HCl, 36%) was from Merck Argentina (Buenos Aires, Argentina). All experiments were performed at 25 °C in 20 mM Tris–HCl pH 7.4 employing triply distilled water, except for experiments of near-infrared luminescence of singlet molecular oxygen, $^1O_2$, for which D_2O (pD 7.4 adjusted with DCl) was used as solvent to improve the signal detection. Compressed ultrapure argon (99.99%) was purchased from Indura SRL (S.M. de Tucumán, Argentina).

2.2. Steady-state spectroscopic measurements

UV–Vis absorption spectra were registered using either a Hewlett Packard 8453 (Palo Alto, CA, USA) or an OceanOptics USB2000 (Dunedin, FL, USA) UV–Vis spectrophotometer. Fluorescence emission measurements were done with a Hitachi F-2500 (Kyoto, Japan) spectrofluorometer, equipped with a red-extended R-928 photomultiplier, and using excitation and emission slits with 5 nm of bandwidth. The fluorescence quantum yield (Φ_F) of RB in BSA solutions was determined by comparison of the integrated fluorescence intensity using as reference the emission of dye in buffer solution ($\Phi_F = 0.018$) [19]; keeping constant the absorbance value at the excitation wavelength (525 nm). Steady-state fluorescence anisotropy r of the RB was determined with a classical L-format and calculated as described elsewhere [20,21].

The steady-state quenching of the intrinsic fluorescence of BSA by addition of RB was studied by excitation at 295 nm. Since RB absorbs light both at the excitation and emission spectral regions of BSA, the observed emission spectra were corrected by the primary and secondary inner filter effects as described before [20,21].

2.3. Time-resolved spectroscopic measurements

Fluorescence emission decays of RB were obtained with a time-correlated single photon counting lifetime spectrofluorometer (Tempro-01 of Horiba Jobin Yvon, Glasgow, UK), using as excitation source an 1 MHz pulsed Nanoled® emitting at 560(±15) nm from Horiba. In order to avoid scattering from the excitation source in the collected dye emission, an interference filter at 543(±10) nm (PIL-1, Schott, Jena, Germany) was placed before the sample holder. The fluorescence emission decays of BSA were collected at 340 nm after excitation with an 1 MHz pulsed Nanoled® emitting at 277(±11) nm. In all cases, the fluorescence emission was monitored through an f/4 monochromator with output slit of 12 nm of bandwidth. The fluorescence intensity decays were fitted with the Fluorescence Decay Analysis Software DAS6® of Horiba Jobin Yvon by deconvolution of the pulse function using the multi-exponential model function,

$$I(t) = \sum_{i=1}^{j} \alpha_i \exp(-t/\tau_{F,i}) \quad (1)$$

where j is the number of single exponential decays, $\tau_{F,i}$ and α_i are the relative fluorescence lifetime intensity amplitude at $t = 0$ of each decay, respectively. In the case of $j > 1$, the average lifetime ($\tau_{F,av}$) was calculated by the following equation, with f_i as the fractional contribution of each decay time to the steady-state intensity.

$$\tau_{F,av} = \sum_{i=1}^{j} f_i \tau_{F,i} \text{ with } f_i = \alpha_i \tau_{F,i} / \sum_{i=1}^{j} \alpha_i \tau_{F,i} \quad (2)$$

Transient absorption spectra of RB were recorded with the m-LFP 112 laser-flash photolysis system of Luzchem Research Inc. (Ottawa, Canada), using as excitation source the second harmonic beam (532 nm, 7 ns fwhm, ~5 mJ/pulse) from a Nd-YAG laser Minilite II of Continuum Inc. (Santa Clara, CA, USA). To minimize degradation of the sample, up to 10-single laser shots were averaged. The transient decays were fitted using a single or double exponential function with the following equation

$$\Delta A_\lambda(t) = \Delta A_\infty + \sum_{i=2} \Delta A_{0,i} \exp(-t/\tau_{T,i}) \quad (3)$$

where $\Delta A_{0,1}$ and $\Delta A_{0,2}$ are the initial difference absorbance associated with each transient of lifetime $\tau_{T,1}$ and $\tau_{T,2}$, respectively, and ΔA_∞ is the ending difference absorbance value. In this case, the average lifetime $\tau_{T,av}$ of the transient species was calculated as:

$$\tau_{T,av} = \frac{\sum_{i=2} \Delta A_{0,i} \tau_{T,i}}{\sum_{i=2} \Delta A_{0,i}} \quad (4)$$

Triplet (Φ_T) and bleaching (Φ_b) quantum yields of RB in BSA solutions were calculated by comparison of the respective transient absorption changes at $t = 0$ (ΔA_0) at each maximum divided by the ground state absorption of the solution at the laser excitation wavelength with that observed for the dye alone in buffer solution, assuming the same extinction coefficient of the transient species without and with protein [12,13].

Transient luminescence detection of singlet molecular oxygen $^1O_2$ at 1270 nm, produced by photosensitization of RB after laser excitation at 532 nm, was performed with a Ge photodiode J16TE2-66G from Teledyne Judson Technology (Montgomeryville, PA, USA). The initial spike in the luminescent signal produced by spurious fluorescence of the dye or scattered laser light was subtracted with the residual signal observed for a RB solution in D_2O

saturated with excess of the singlet oxygen quencher NaN_3. As in the LFP experiments, to avoid sample degradation and/or possible interference of $^1O_2$-mediated oxidation products, up to 10-single luminescent signal of $^1O_2$ were averaged. The transient signal was fitted with the following bi-exponential function,

$$I_\Delta(t) = I_{\Delta,0}\frac{\tau_{\Delta,d}}{(\tau_{\Delta,r}-\tau_{\Delta,d})}(e^{-t/\tau_{\Delta,r}} - e^{-t/\tau_{\Delta,d}}) \quad (5)$$

where $I_{\Delta,0}$ is the initial luminescence intensity, and $\tau_{\Delta,r}$ and $\tau_{\Delta,d}$ are the rise and decay times of $^1O_2$, respectively. The singlet oxygen formation quantum yield (Φ_Δ) by RB in presence of BSA was determined by comparison of the fitted $I_{\Delta,0}$ values with that observed for RB alone in deuterated solution ($\Phi_\Delta = 0.76$), after correction by difference in the ground state absorption of the dye at 532 nm between sample and reference solutions [12].

All experiments were performed at 25(±1) °C in fused silica cells under air-saturated aqueous or deuterated solutions. Additional LFP experiments in Argon-saturated solutions were performed by soft bubbling of ultrapure Ar during 30 min to avoid foam formation in BSA solutions.

3. Results and discussion

3.1. Spectroscopic and photophysical consequences of RB binding to BSA

The spectroscopic properties of RB and its derivatives in solution are dependent on both self-interactions of the dye and solvent properties [15]. In addition, interactions of RB with supra- and macromolecular assemblies, such as polyelectrolytes [17], micelles [22], and proteins [23] strongly modulates its spectral properties, in particular upon binding to serum albumins [12,23–26].

Fig. 1A shows the modification of the visible absorption band of 10 μM RB in 20 mM Tris–HCl buffer solution at pH 7.4 with increasing concentrations of BSA. The global changes observed are an initial strong hypocromic and band broadening followed of a hyperchromic and red shift of the visible band of the dye, as previously reported [24,25]. Furthermore, in this work we remark that the initial hypochromic effect is accompanied by a parallel increase of both the full width half maximum (FWHM) and the shoulder-to-maximum absorption ratio (S/M) of the visible absorption band of RB up to [BSA] ≈ 1.5 μM, Fig. 1B. However, above this protein concentration, both FWHM and S/M progressively decrease to similar values than those observed for monomeric RB in non-hydrogen bonding and less polar solvents [15]. This spectral shape modification is also accompanied by a sudden red shift of ≈12 nm of the absorption maximum λ_{ab}^{max}, with an apparent midpoint shift coincident with the maximum value observed for the variation of FWHM and S/M.

In turns, the fluorescence emission spectrum of RB obtained with excitation at the shoulder band around 522 nm, where the absorption of the solutions almost did not changed by addition of the albumin, also was largely dependent on the protein concentration, Fig. 2A. The fluorescence band of the dye initially was quenched by adding BSA, effect that was strongly reverted at larger protein concentrations. The fluorescence maximum of RB at ≈572 nm was almost unchanged at [BSA] < 1.5 μM, but with increasing BSA concentration a final red shift of ≈10 nm was evidenced.

Fig. 2B compares the variation of the fluorescence quantum yield Φ_F and steady-state anisotropy r with the albumin concentration, and it can be observed that both parameters initially decreases up to a minimum value around [BSA] ≈ 1.5 μM, but by increasing the albumin concentration a large increment up to limiting values of $\Phi_F = 0.12 \pm 0.01$ and $r = 0.365 \pm 0.05$ were observed.

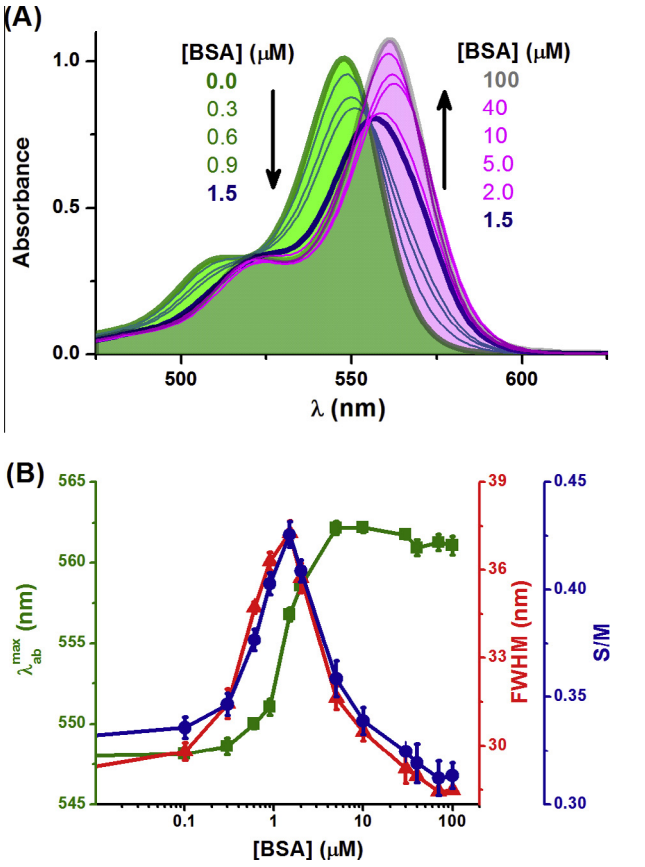

Fig. 1. (A) Visible absorbance spectral changes produced in 10 μM RB in 20 mM Tris–HCl buffer solutions at pH 7.4 by the addition of bovine serum albumin (BSA). (B) Variation with the analytical protein concentration [BSA] of the absorbance maximum λ_{ab}^{max} (■), full width half maximum FWHM of absorption band (▲), and shoulder-to-maximum absorbance ratio S/M (●) of the dye.

The fluorescence decay of RB at [BSA] ⩽ 1.5 μM showed mono-exponential behavior with almost constant lifetime of 69 ± 7 ps, as expected for monomeric RB in aqueous media [27], (see Fig. S1 of Supporting Information). Nevertheless, as the albumin concentration was increased above ≈2 μM, the fluorescence decay of RB turned bi-exponential with a sudden increases of both individual lifetimes up to final mean values of 327 ± 30 ps (≈68%) and 897 ± 45 ps (≈32%), as it is shown in Fig. S1. This complex decay for RB in presence of albumin excess indicates that singlet excited states of the dye $^1RB^*$ senses a heterogeneous nanoenvironment, as it is discussed below. In order to compare the fluorescence dynamic behavior of RB with the fluorescence steady-state parameters Φ_F and r, Fig. 2B also shows the dependence with the BSA concentration of the average fluorescence lifetime $\tau_{F,av}$, as calculated with Eq. (2). Despite of $\tau_{F,av}$ is an intensity weighted parameter [20], it can be observed a sigmoidal-like increases of this parameter with the albumin concentration with a constant value of up to 509 ± 20 ps at [BSA] > 10 μM. A similar result was also observed for the RB-HSA system [12]. A lifetime enhancement of RB is typically observed in non-polar and non-hydrogen bonding media [27], therefore, it can be assumed that at large excess of albumin the dye is bound into a hydrophobic site of the protein, where water molecule are excluded.

The observed changes on both spectroscopic and photophysical properties of RB can be explained in terms of the occurrence of different dye binding processes as a function of the albumin concentration. At low BSA concentrations, *e.g.* <1.5 μM, the larger molar excess of dye relative to protein can drive to the nonspecific

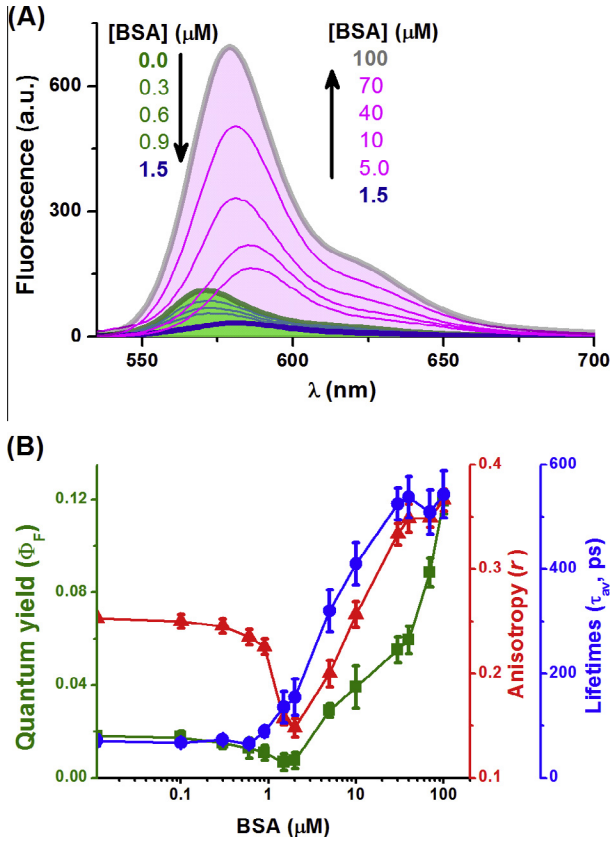

Fig. 2. (A) Fluorescence emission changes produced in 10 μM RB in 20 mM Tris–HCl buffer solutions at pH 7.4 by the addition of bovine serum albumin (BSA). Excitation was fixed at 522 nm. (B) Variation with the analytical protein concentration [BSA] of the fluorescence quantum yield (Φ_F, ■), steady state emission anisotropy (r, ▲), and average fluorescence lifetime (τ_{av}, ●) of RB.

binding of several dye molecules onto a single protein, represented by the pseudophase equilibrium of Eq. (6).

$$RB_{free} + BSA \rightleftarrows RB_{bound} \quad K_b^* = \frac{[RB_{bound}]}{[RB_{free}][BSA]} \tag{6}$$

As a consequence of the binding of several RB molecules per albumin molecule, the local concentration of the dye largely increases, favoring the occurrence of dimers or larger dye aggregates onto the protein. This colocalization effect of the dye can explain the initial increment of both FWHM and *S*/*M* ratio of the absorption band of RB, Fig. 1B, since the absorption spectrum of the RB dimer shows hypochromic effect by strong decreases in its oscillator strength, slight broadening, and larger relative absorption of the blue-shifted transition around 525 nm increasing the *S*/*M* ratio as compared with its monomer [16]. This phenomena has been already observed by local concentration increases of RB in both cationic and zwitterionic surfactants [22], polyelectrolyte multilayers [28], colloidal particles [18], and in Type-I human collagen [29]. The formation of dye aggregates onto the albumin molecule also explains the observed initial decreases of both Φ_F and r of RB, as well as the monoexponential behavior of the fluorescence decay of the dye (≈70 ps) at low albumin concentration, Fig. 2B. Under dye aggregation conditions the prevalence of efficient "static" quenching mechanism of the excited singlet state of RB is allowed, probably by energy-transfer through the multiple dye molecules in the protein, decreasing fluorescence quantum yield and also enhancing fluorescence depolarization [30]. In this case, only the remaining free RB molecules contribute to the dye emission intensity and decay.

However, the increases of the BSA concentration between 2 and 10 μM produces the sudden spectral red shift of both absorption and fluorescence bands, together with the band narrowing, diminution of *S*/*M* ratio, and recovery of photophysical parameters , Figs. 1 and 2. All together, these results indicate the destruction of the intra-protein dye aggregates in favor of the localization of single or non-aggregated dye molecules per protein. This "compartmentalized dilution" process of RB is produced by the shifting to the left of the non-specific equilibrium represented by Eq. (6) by an extra equilibrium between a free dye molecule and an unoccupied protein site, forming an adduct RB:BSA with a binding constant K_b, Eq. (7).

$$RB_{free} + BSA_{unoccupied} \rightleftarrows RB:BSA \quad K_b = \frac{[RB:BSA]}{[RB_{free}]([BSA] - [RB:BSA])} \tag{7}$$

The equilibrium of Eq. (7) is favored when [BSA] ≫ [RB], and under this condition, a one to one dye-protein complex can be formed [12,24], as suggested the presence of an isosbestic point ~555 nm in the absorption spectra of RB at [BSA] < 40 μM, Fig. 1A. Above this protein concentration the isosbestic point is partially lost probably by protein aggregation effects [31]. Therefore, for the protein concentration range where the isosbestic point is hold, the blue- and red-shifted bands can be assigned to the presence of free ($[RB]_{free}$) and bound ($[RB]_{bound}$) dye species, respectively. In this framework, $[RB]_{bound} = f_b \times [RB]_0$ with f_b as the fraction of the dye bound to the protein and $[RB]_0$ is the analytical dye concentration. The f_b can be estimated using the absorbance value at 561 nm of RB as a function of the BSA concentration as $f_b = (A - A_f)/(A_b - A_f)$, where A_f and A_b are the absorbance values of RB in buffer and when it is totally bound to the protein, respectively. The latter value was estimated by extrapolation of the sample absorbance to "infinite" BSA concentration [12]. Thus, from the estimated f_b values, the binding isotherm can be constructed by plotting the average number of dye molecules per protein ($n = [RB]_{bound}/[BSA]$) *vs.* the free dye concentration $[RB]_{free} = (1 - f_b)[RB]_0$, Fig. 3. The calculated binding isotherm of Fig. 3 showed a sigmoidal-like shape indicating a complex dye association mechanism [32]. In the present case, this behavior can be assigned to the presence of the sequential equilibriums of Eqs. (6) and (7), which relative contribution of each of them strongly depends on the n value. Thus, the complete binding isotherm of Fig. 3 was analyzed using the two-terms modified Hill Eq. (8) [33], where n^*_{max}, ν^*_H, and K^*_b represent the maximum average number of bound dye molecule per protein, the cooperative Hill factor, and the binding constants for equilibrium 6, respectively, while n_{max}, ν_H, and K_b are those for equilibrium 7.

$$n = \frac{n^*_{max}[RB]_{free}^{\nu^*_H}}{(1/K^*_b)^{\nu^*_H} + [RB]_{free}^{\nu^*_H}} + \frac{n_{max}[RB]_{free}^{\nu_H}}{(1/K_b)^{\nu_H} + [RB]_{free}^{\nu_H}} \tag{8}$$

The best fitting of the binding isotherm with Eq. (8) is represented by the solid sigmoidal line in Fig. 3, giving the following set of binding parameters: $K_b = 0.15 \pm 0.02\ \mu M^{-1}$, $n_{max} = 1.1 \pm 0.4$, $\nu_H = 0.8 \pm 0.3$; and $K^*_b = 0.23 \pm 0.05\ \mu M^{-1}$, $n^*_{max} = 5.6 \pm 0.2$, $\nu^*_H = 2.6 \pm 0.3$, respectively. Within the statistical error bars, the first set of fitted parameters for equilibrium 7 modeled quite well a binding process with stoichiometry 1:1, as $n_{max} \approx 1$, and without noticeable cooperative effects ($\nu_H \approx 1$) [32,33]. This binding process is represented in the initial lineal portion of the binding isotherm where $n < 1$. To confirm this result, we calculated also K_b by applying the Encinas–Lissi (E–L) method [34,35], using the quenching efficiency of the intrinsic Trp-like fluorescence of the protein by RB as a function of the BSA concentration in the range between 1.7 and 21 μM to minimize the effect of self-protein aggregation. As briefly described in the Supporting Information, the E–L method allows the estimation of n as a function of $[RB]_{free}$ independently of both the binding and

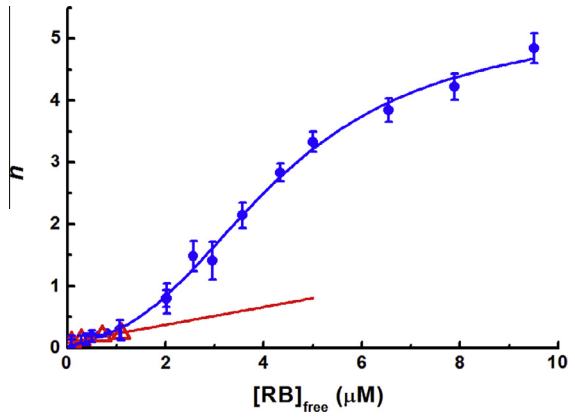

Fig. 3. (●) Isotherm curve for the binding of RB to BSA in 20 mM Tris–HCl buffer solutions at pH 7.4 at 25 °C, calculated from absorbance changes of RB at 561 nm, and (△) isotherm calculated by protein quenching by RB (Encinas–Lissi method [34]). Solid sigmoidal line represents the non-lineal fitting of the whole isotherm curve with the modified Hill Eq. (8), while the solid linear line is the lineal regression of the data from fluorescence quenching experiments. (For interpretation of the references to colour in this figure legend, the reader is referred to the web version of this article.)

quenching mechanisms. Fig. S2 of Supporting Information shows the Stern–Volmer plots for the quenching data and the final set of *n vs.* $[RB]_{free}$ values were also included in Fig. 3(open red[1] triangles). It can be observed that this set of independent data was coincident with those of the lineal portion of the binding isotherm calculated with the absorbance changes, and from the lineal regression of the fluorescence quenching data $K_b = n/[RB]_{free} = 0.14 \pm 0.01\ \mu M^{-1}$ was obtained. Therefore, considering both binding analysis at $n < 1$, it can be assumed the formation of a one-to-one RB:BSA adduct in neutral Tris–HCl buffer with $K_b = 0.15 \pm 0.01\ \mu M^{-1}$. Abuin et al. [24] have applied the classical Benesi–Hildebrand (B–H) treatment using the absorption changes of RB produced by BSA to obtain $K_b \approx 0.35\ \mu M^{-1}$ in neutral phosphate buffer media. Their results confirmed that the binding is practically dominated by hydrophobic driving force, since the presence of 8 M urea strongly reduces K_b, while ionic strength modifications of the buffer solution did not change it significantly [24].

On the contrary, the fitted parameters associated with the pseudophase equilibrium 6, indicate that this process is governed by a positive cooperative binding effect, as $\nu_H^* = 2.6$ [32], and that each BSA molecule is able to accommodate up to approximately six dye molecules ($n_{max}^* = 5.6 \pm 0.2$). Recently, it has been reported that almost ten RB molecules can be adsorbed onto the surface of free form of recombinant Type-I human collagen, with the formation of dimer-like aggregates of the dye [29]. Therefore, non-specific binding of multiple dyes molecules onto BSA at $n > 1$ can allow dye self-interactions responsible of the initial spectroscopic and photophysical changes produced at low BSA concentration as described above.

Accordingly with $K_b = 0.15\ \mu M^{-1}$, it can be expected the quantitative formation of the RB:BSA adduct at $n < 0.2$ (*i.e.* [BSA] > 30 μM). Under these conditions all spectroscopic (*e.g.* FWHM, *S*/*M*, λ_{ab}^{max}, and λ_F^{max}) and photophysical (*e.g.* Φ_F and $\tau_{F,av}$) properties of RB resembled to those observed for the monomeric dye in organic solvents with lower hydrogen-bonding capacity and polarity than water [27,36]. Furthermore, all these parameters for the RB:BSA adduct were very similar to those observed for the interaction of RB with human serum albumin (HSA), despite of the larger K_b value observed for the formation of the RB:HSA adduct [12]. These results suggest that in both albumins the dye bounds into a hydrophobic protein pocket with similar nanoenvironmental properties, but with lower affinity for BSA. In the case of HSA, dansyl-probes displacement by RB experiments demonstrated that the dye preferably binds to the hydrophobic subdomain IIA (or Sudlow's site I) of the protein [12,13], as it is generally accepted for bulky heterocyclic anions [14]. Considering that BSA shares ≈76% of the amino acidic sequence homology with HSA [14], it can be also expected the binding of RB into site I of BSA.

Fig. 2B shows that the limiting RB anisotropy value with the protein concentration was very closer to the fundamental anisotropy reported for the dye, *e.g.* $r_0 = 0.373$ [37], indicating that the RB molecule is rigidly encased in the site I of the protein. The anisotropy increases for RB bound in BSA should be the result of a much longer rotational correlation lifetime τ_c than the averaged fluorescence lifetime of the dye, *i.e.* $\tau_c \gg \tau_{F,av}$. In fact, a time-resolved anisotropy measurement of RB under protein concentration to assure >95% of dye bound to BSA yielded $\tau_c = 44 \pm 5$ ns, as calculated assuming a depolarization exponential decay expected for a spherical rotor (Fig. S3, Supporting Information). This τ_c value for RB is almost two-order of magnitude larger than $\tau_{F,av}$ and very closer to the reported values for the rotational depolarization of serum albumins in water at 25 °C [38], meaning that the depolarization decay of RB bound to BSA is almost governed by the rotational diffusion of the whole protein, confirming the tight binding of the dye molecule into the hydrophobic site I of the protein.

Under conditions of quantitative binding of RB to BSA, e.g. $n \ll 1$, the fluorescence decay of the dye showed a bi-exponential behavior as mentioned before, indicating a heterogeneous population of the singlet excited state of the dye, $^1RB^*$. However, the decay-associated emission spectra of both decay component of RB obtained by global fitting analysis of the fluorescence decays between 570 and 700 nm were the same than the steady-state emission spectrum of the dye obtained under the same condition (Fig. S4, Supporting Information). This result indicates that both populations of $^1RB^*$ sense almost the same global intraprotein nanoenvironment, ruling out the binding of the dye into different protein sites. Therefore, the bi-exponential decay of $^1RB^*$ could be associated with subtle distance modifications between the bound dye and the surrounding amino acids due to the existence of different BSA conformers in solution [14], modifying the degree of ultra-fast charge-transfer quenching of $^1RB^*$ by interacting amino acids of the binding site [39].

3.2. Photosensitizing properties of RB bound to BSA

Fig. 4 compares the transient absorption decays obtained by laser-flash photolysis experiments of the excited triplet state of RB ($^3RB^*$) monitored at 620 nm in the presence of 0.1 μM and 50 μM of BSA in both argon- and air-saturated buffer solutions.

The band maximum corresponding to the negative bleaching band of the dye showed similar kinetic behavior than $^3RB^*$ (data not shown), but it was progressively shifted to the red in the same fashion that λ_{ab}^{max} in the visible absorption spectra of the ground-state of RB, Fig. 1. Under protein concentration conditions where the variation of the average number of dye molecules per protein was $3 < n < 6$, both triplet and bleaching transient absorption signals of RB decayed almost monoexponentially with lifetimes of $\tau_T \approx 70$ μs and 3 μs in Ar- and air-saturated solutions, respectively, as occurred for the dye alone in buffer solutions. However, the initial absorption difference ΔA_0, which is proportional with the amount of transient excited state formed, was strongly reduced by the addition of small amount of BSA (Fig. S5 of Supporting Information). These results agree with the non-specific multiple binding dye molecules per albumin molecule effect, producing large static quenching of the RB excited states by formation of intra-protein

[1] For interpretation of color in Fig. 3, the reader is referred to the web version of this article.

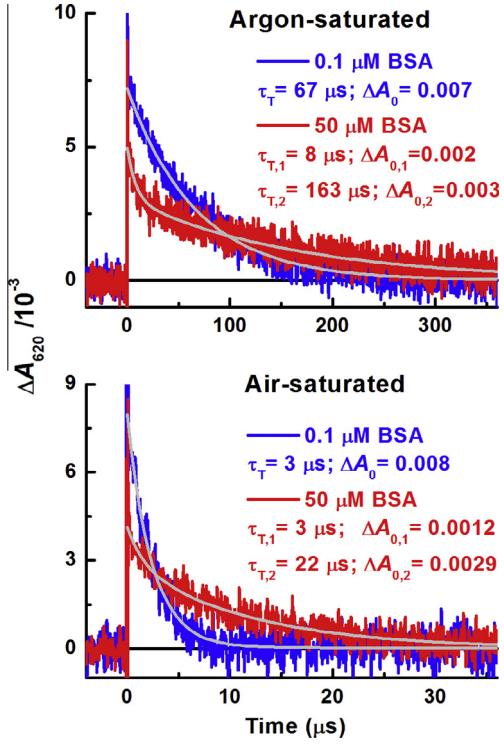

Fig. 4. Transient absorption decay of the excited triplet state of 10 μM RB monitored at 620 nm as obtained after laser excitation at 532 nm (4 mJ/pulse, 7 ns fwhm) in presence of 0.1 μM (blue lines) and 50 μM (red lines) BSA, both in argon and air-saturated 20 mM Tris–HCl buffer solutions at pH 7.4. Gray solid lines represent the fitting of the signals with Eq. (3), and the fitting parameters are also indicated. (For interpretation of the references to colour in this figure legend, the reader is referred to the web version of this article.)

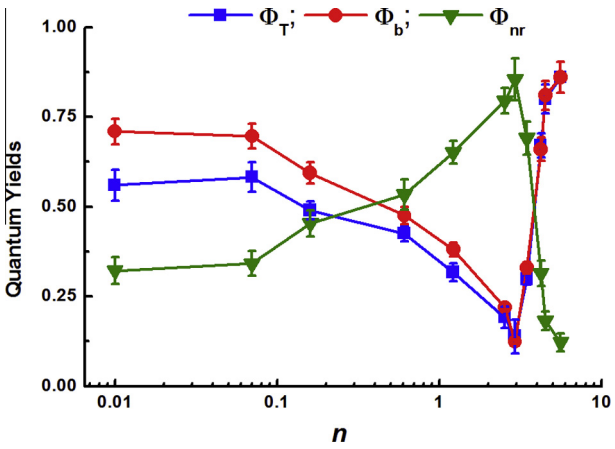

Fig. 5. Variation of the quantum yield of triplet formation Φ_T (■); ground-state bleaching Φ_b (●); and internal conversion Φ_{ic} (▼) as function of the average number of bound dyes molecules per protein $n = [RB]_b/[BSA]$.

aggregates of the dye, as discussed before. However, at higher BSA concentrations where $n < 1$, the transient signals became bi-exponential and the ΔA_0 was also partially recovered, as it is shown in Fig. 4. Again, as described at the end of the previous section for the dynamic behavior of $^1RB^*$, the bi-exponential decay the triplet excited state $^3RB^*$ can also be associated with the presence of different BSA conformers in solution. Under these conditions, the apparent average transient lifetimes values were $\tau_{T,av} = 102 \pm 5$ μs and 27 ± 2 μs in argon and air-saturated solutions, respectively. In all cases the shorter transient lifetime component represented about 30–40% of the decay (Fig. S5 of Supporting Information).

Fig. 5 shows the variation of the quantum yield of triplet state formation (Φ_T), ground state bleaching (Φ_b), and internal conversion ($\Phi_{ic} = 1-\Phi_F-\Phi_T$) *vs.* the average number of dye molecules per protein (i.e. $n = [RB]_{bound}/[BSA]$), the latter one as extracted from the binding isotherm of Fig. 3. As mentioned above, under high dye loading conditions both Φ_T and Φ_b values decreased up to $\approx 0.12 \pm 0.02$ at $n = 3$, condition were > 50% of dye molecules are bound to the protein. Thus, the static quenching of the excited states of RB by colocalization of dye molecules into the protein was maximized, as indicated by the largest quantum yield value for non-radiative relaxation process, Φ_{ic}.

On the other hand, at $n \ll 1$, the RB:BSA adduct is formed quantitatively and the bleaching and triplet quantum yields were recovered up to $\Phi_b = 0.71 \pm 0.03$ and $\Phi_T = 0.56 \pm 0.06$, respectively, which are lower values than for the free RB in buffer ($\Phi = 0.86$). This fact together with the splitting between Φ_b and Φ_T could be the result of prompt quenching reactions of a fraction of $^3RB^*$ with surrounding aminoacids of the binding site I of BSA. In such a case, this assumption agrees with the bi-exponential decay behavior of $^3RB^*$ for the adduct, e.g. $\tau_{T,1} = 8 \pm 1$ μs and $\tau_{T,2} = 163 \pm 9$ μs in Ar-saturated solutions, Fig. 4. Moreover, after prolonged irradiation times of RB:BSA adduct, about 5–8% of the dye was bleached, suggesting that a small fraction of RB triplets are reactive, probably by charge-transfer reactions with nearby electron-donor aminoacids (Type I mechanism). However, the transient spectrum of the RB:BSA adduct in the time range between ns to μs did not show any new transient decay assigned to radical ion species, signifying that ultra-fast recombination of primary radical ions is produced in the rigid binding site I [39].

On the other hand, under aerobic conditions, both bleaching and triplet transient signals were shortened without significant modification of both Φ_b and Φ_T. The influence of the protein nanoenvironment on the interaction of $^3RB^*$ with dissolved molecular oxygen O_2 can be evaluated by the quenching efficiency calculated as $\eta_q^{O_2} = 1 - \tau_{T,av}^{Air}/\tau_{T,av}^{Ar}$. In buffer solution and in absence of protein $\eta_q^{O_2} = 0.96 \pm 0.02$ and decreases to 0.74 ± 0.03 under conditions of quantitative formation of the RB:BSA adduct (e.g. $n \ll 1$) despite of the longer average lifetime of the $^3RB^*$ bound to the protein. Considering a homogenous distribution of O_2 concentration in air-saturated protein solutions, *i.e.* $[O_2] = 0.27$ mM, the decline of $\eta_q^{O_2}$ for the RB:BSA adduct represents almost one-order of magnitude decreases of the average quenching rate constant $^3RB^*$ by O_2, i.e. $k_{q,av}^{O_2} \approx 10^8$ $M^{-1}s^{-1}$, as it was previously observed for RB bound to HSA [12]. Accordingly with the steady state and dynamic emission anisotropy results described before, the local rigidity of the binding site of RB can impose a barrier to the free diffusion of O_2 from the bulk buffer. Nevertheless, despite of this diffusional barrier, the quenching of $^3RB^*$ bound to BSA by O_2 generates singlet molecular oxygen $^1O_2$, as directly detected by the transient luminescence at 1270 nm after laser excitation of the dye at 532 nm in air-saturated deuterated buffer solutions, Fig. 6A. As compared with the $^1O_2$ luminescence signal obtained in the absence of BSA, the addition of protein reduces the initial intensity ($I_{\Delta,0}$) and increases the rise time ($\tau_{\Delta,r}$) of $^1O_2$. The latter one also corresponds to the decay time of $^3RB^*$ in air-saturated conditions ($\tau_{T,av}^{Air}$). Due to that the signal-to-noise ratio of the $^1O_2$ luminescence traces are not optimal, in order to minimize the fitting error by using Eq. (5), the $\tau_{T,av}^{Air}$ ($\equiv\tau_{\Delta,r}$) value obtained by laser-flash photolysis experiments was used as fixed parameter in the fitting procedure allowing a more accurate calculation of both $I_{\Delta,0}$ and decay time ($\tau_{\Delta,d}$) of $^1O_2$. After this procedure, the $\tau_{\Delta,d}$ value steadily decreased from 67 ± 2 μs to 19 ± 4 μs by increasing the BSA concentration up to 50 μM, indicating a dynamic overall

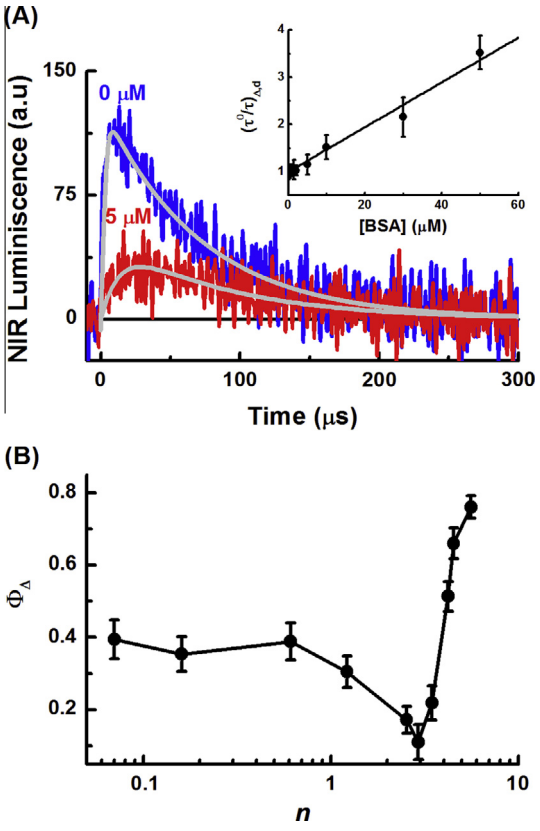

Fig. 6. (A) Transient luminescence signals of singlet molecular oxygen at 1270 nm obtained after photosensitization of 10 μM RB with laser excitation at 532 nm (4 mJ/pulse) in air-saturated D_2O solutions in absence (blue line) and presence of 5 μM BSA (red line). Gray lines represent signal fitting with Eq. (6). Inset: Stern–Volmer plot for the dynamic quenching of $^1O_2$ by BSA in neutral D_2O solutions. (B) Variation of the quantum yield for $^1O_2$ formation (Φ_Δ) vs. the average number of RB molecules per BSA (n). (For interpretation of the references to color in this figure legend, the reader is referred to the web version of this article.)

quenching (physical + chemical) of $^1O_2$ by BSA, which total bimolecular quenching rate constant k_Q^{BSA} was calculated according to the Stern–Volmer Eq. (9).

$$\left(\frac{\tau^0}{\tau}\right)_{\Delta,d} = 1 + \tau_{\Delta,d}^0 k_Q^{BSA}[BSA] \quad (9)$$

The inset of Fig. 6A shows the lineal fitting of Eq. (9), and from the slope value the $k_Q^{BSA} = 7.2(\pm 0.4) \times 10^8\ M^{-1}\ s^{-1}$ was obtained. This quenching rate constant value is similar to those reported for the quenching of $^1O_2$ by HSA using as photosensitizer either methylene blue (MB) that is bound to the site II of the protein [13] or phenalen-1-one-2-sulfonic acid (PNS) that is mostly located in the bulk buffer [40]. The k_Q^{BSA} value falls in the range of $\sim 10^8$–$10^9\ M^{-1}$ - s^{-1} as reported for several proteins [40,41], but it is one- or two order of magnitudes larger than for the quenching of $^1O_2$ by electron-rich free amino acids as Trp, Tyr, His, Met, and Cys [42]. This means that k_Q^{BSA} reflects the quenching contribution of several amino acids in the protein, probably those more exposed to the solvent. The chemical reaction of $^1O_2$ with the amino acids induces oxidative modification of the protein by increasing the formation of carbonyl and peroxides derivatives at the protein surface [6,12,43,44]. Furthermore, independently of the $^1O_2$ generation site, *i.e.* extra- or intraprotein, the radial distance traveled by $^1O_2$ during a travel time t can be approximately calculated as $d = (6Dt)^{1/2}$ [45], where D is the diffusion coefficient of $^1O_2$ in the media. Considering that $t \approx 5\tau_{\Delta,d} = 5 \times (3\ \mu s)$ and $D = 2 \times 10^{-5}\ cm^2/s$ in water at room temperature [46], it can be estimated that $d \approx 500$ nm, which is distance several orders of magnitude larger that the protein size, allowing the free diffusion of $^1O_2$ generated into a protein that bears a RB molecule to the bulk buffer and its interaction during its lifetime with different empty BSA molecules.

In turns, the fitted $I_{\Delta,0}$ values allows the estimation of the quantum yield of $^1O_2$ formation Φ_Δ (see Section 2), and those values are plotted as a function of n in Fig. 6B. Once more, the Φ_Δ value of RB decreases in similar fashion than for Φ_T in the region of high dye occupancy in the protein, i.e. $n > 3$. However, the recovery of Φ_Δ under conditions of low dye occupancy ($n \ll 1$) was only ≈50% of the initial value in the buffer solution, $\Phi_\Delta = 0.76$. This quantum yield difference cannot be assigned to lower efficiency of $^3RB^*$ quenched by O_2 that generates $^1O_2$, *i.e.* $S_\Delta = \Phi_\Delta/(\eta_q^{O_2}\Phi_T)$, since it was almost the same in bulk buffer and for RB:BSA solutions ($S_\Delta \approx 0.92$). Therefore, the reduced Φ_Δ for the RB:BSA adduct should be consequence of the compartmentalization effect imposed by the site I of the protein, since under this condition the combined contribution of the reduction of the amount of $^3RB^*$ by static quenching due to surrounding aminoacids and of the decreased free diffusion of ground state O_2 to quench the $^3RB^*$ into the protein play a role in the intra-protein photosensitization of $^1O_2$. Nevertheless, the present results suggest that RB encased in BSA is almost 10- and 100-times more efficient $^1O_2$ generator than miniSOG [10,11] and GFP [8] proteins, respectively.

4. Conclusions

The present work demonstrates the relevance of self-interactions and compartmentalization effects of xanthene sensitizers bound to serum albumins, which modulate both spectroscopic and photophysical properties of RB. At high molecular excess of RB relative to BSA, the non-specific binding of up to ≈6 molecules of dye per protein is produced. Under conditions where the average number of dye molecules per BSA (n) was ranging between 3 and 6, the formation of self-aggregates of RB into the protein allows efficient static quenching of excited states of RB that precludes the photosensitization of $^1O_2$. Conversely, under conditions where $n < 1$, the specific binding of one RB molecule to the hydrophobic Sudlow's site I of BSA is produced to form a RB:BSA adduct with a constant binding $K_b \approx 0.15\ \mu M^{-1}$. The spectroscopic and photophysical properties of the dye forming the RB:BSA adduct are dominated by the environmental and amino acid composition of the hydrophobic nanocavity. The main effects are the exclusion of hydrogen bonding interactions with external water molecules and static quenching process of the excited states of RB by surrounding amino acids, which avoids the total recovery of the photosensitizing properties of the dye. Regardless of the diffusive barrier for the quenching of the triplet excited state of the bound dye by dissolved oxygen, the RB:BSA adduct is able to photogenerate $^1O_2$ with relatively high quantum yield (≈0.35), a value between 10- and 100-times larger than for other protein singlet oxygen generators, such as miniSOG and GPF [8,11], suggesting the suitability of this sensitizer-protein encased supramolecule for PDT applications. Finally, the BSA itself is able to quench $^1O_2$ with an overall quenching rate constant of $7.2 \times 10^8\ M^{-1}\ s^{-1}$, which yields a quenching efficiency of $^1O_2$ in aqueous media of ≈0.56 considering a serum albumin concentration ≈600 μM under physiological conditions. Therefore, it can expect that less of the half of $^1O_2$ generated is able to interact with other target molecules in plasma solutions.

Acknowledgements

We specially thank Ricardo A. Mignone for technical assistance and Dr. Inés Abatedaga of CITSE-UNSE for helping in the analysis of

the pdb structure of BSA. This research was supported by Argentinean grants of the Consejo Nacional de Investigaciones Científicas y Técnicas (CONICET- PIP 0374/12), Agencia de Promoción Científica y Tecnológica (ANPCyT- PICT 2012-2666), and Universidad Nacional de Santiago del Estero (UNSE-CICyT 23A/162). N.M.A. and M.B.E.T thanks CONICET for doctoral and postdoctoral fellowships, respectively. V.R., F.E.M.V., and C.D.B. are research members of CONICET.

Appendix A. Supplementary material

Supplementary data associated with this article can be found, in the online version, at http://dx.doi.org/10.1016/j.jphotobiol.2014.09.014.

References

[1] M.C. DeRosa, R.J. Crutchley, Photosensitized singlet oxygen and its applications, Coord. Chem. Rev. 233 (2002) 351–371.
[2] J. Wahlen, D.E. De Vos, P.A. Jacobs, P.L. Alsters, Solid materials as sources for synthetically useful singlet oxygen, Adv. Synth. Catal. 346 (2004) 152–164.
[3] C.A. Robertson, D.H. Evans, H. Abrahamse, Photodynamic therapy (PDT): a short review on cellular mechanisms and cancer research applications for PDT, J. Photochem. Photobiol. B: Biol. 96 (2009) 1–8.
[4] M.J. Garland, C.M. Cassidy, D. Woolfson, R.F. Donnelly, Designing photosensitizers for photodynamic therapy: strategies, challenges and promising developments, Future Med. Chem. 1 (2009) 667–691.
[5] Y. Wang, B. Han, R. Shi, L. Pan, H. Zhang, Y. Shen, C. Li, F. Huang, A. Xie, Preparation and characterization of a novel hybrid hydrogel shell for localized photodynamic therapy, J. Mater. Chem. B 1 (2013) 6411–6417.
[6] E. Alarcon, A.M. Edwards, A.M. Garcia, M. Munoz, A. Aspee, C.D. Borsarelli, E.A. Lissi, Photophysics and photochemistry of zinc phthalocyanine/bovine serum albumin adducts, Photochem. Photobiol. Sci. 8 (2009) 255–263.
[7] R. Ruiz-Gonzalez, J.H. White, M. Agut, S. Nonell, C. Flors, A genetically-encoded photosensitiser demonstrates killing of bacteria by purely endogenous singlet oxygen, Photochem. Photobiol. Sci. 11 (2012) 1411–1413.
[8] X. Ragàs, L.P. Cooper, J.H. White, S. Nonell, C. Flors, Quantification of photosensitized singlet oxygen production by a fluorescent protein, ChemPhysChem 12 (2011) 161–165.
[9] Y.B. Qi, E.J. Garren, X. Shu, R.Y. Tsien, Y. Jin, Photo-inducible cell ablation in Caenorhabditis elegans using the genetically encoded singlet oxygen generating protein miniSOG, Proc. Natl. Acad. Sci. USA 109 (2012) 7499–7504.
[10] R. Ruiz-González, A.L. Cortajarena, S.H. Mejias, M. Agut, S. Nonell, C. Flors, Singlet oxygen generation by the genetically encoded tag miniSOG, J. Am. Chem. Soc. 135 (2013) 9564–9567.
[11] F.M. Pimenta, R.L. Jensen, T. Breitenbach, M. Etzerodt, P.R. Ogilby, Oxygen-dependent photochemistry and photophysics of "MiniSOG", a protein-encased flavin, Photochem. Photobiol. 89 (2013) 1116–1126.
[12] E. Alarcon, A.M. Edwards, A. Aspee, C.D. Borsarelli, E.A. Lissi, Photophysics and photochemistry of rose bengal bound to human serum albumin, Photochem. Photobiol. Sci. 8 (2009) 933–943.
[13] E. Alarcon, A.M. Edwards, A. Aspee, F.E. Moran, C.D. Borsarelli, E.A. Lissi, D. Gonzalez-Nilo, H. Poblete, J.C. Scaiano, Photophysics and photochemistry of dyes bound to human serum albumin are determined by the dye localization, Photochem. Photobiol. Sci. 9 (2010) 93–102.
[14] T. Peters, All about Albumin Proteins, Academic Press, New York, 1996.
[15] D.C. Neckers, Rose bengal, J. Photochem. Photobiol. A: Chem. 47 (1989) 1–29.
[16] O.M. Valdes-Aguilera, D.C. Neckers, Aggregation phenomena in xanthene dye, Acc. Chem. Res. 22 (1989) 171–177.
[17] M. Mirenda, L.E. Dicelio, E.S. Roman, Effect of molecular interactions on the photophysics of Rose Bengal in polyelectrolyte solutions and self-assembled thin films, J. Phys. Chem. B 112 (2008) 12201–12207.
[18] H.B. Rodriguez, M.G. Lagorio, E.S. Roman, Rose bengal adsorbed on microgranular cellulose: evidence on fluorescent dimers, Photochem. Photobiol. Sci. 3 (2004) 674–680.
[19] G.R. Fleming, A.W.E. Knight, J.M. Morris, R.J.S. Morrison, G.W. Robinson, Picosecond fluorescence studies of xanthene dyes, J. Am. Chem. Soc. 99 (1977) 4306–4311.
[20] J.R. Lakowicz, Principles of Fluorescence Spectroscopy, third ed., Springer Science+Business Media, LLC, Singapore, 2006.
[21] J.M. Villegas, L. Valle, F.E. Morán Vieyra, M.R. Rintoul, C.D. Borsarelli, V.A. Rapisarda, FAD binding properties of a cytosolic version of Escherichia coli NADH dehydrogenase-2, Biochim. Biophys. Acta (BBA) Proteins Proteomics 144 (2014) 576–584.
[22] P. Bilski, R.N. Holt, C.F. Chignell, Premicellar aggregates of rose bengal with cationic and zwitterionic surfactants, J. Photochem. Photobiol. A Chem. 110 (1997) 67–74.
[23] Y.Z. Zhang, H. Gorner, Photoprocesses of xanthene dyes bound to lysozyme or serum albumin, Photochem. Photobiol. 85 (2009) 677–685.
[24] E. Abuin, A. Aspée, E. Lissi, L. León, Binding of rose bengal to bovine serum albumin, J. Chilean Chem. Soc. 52 (2007) 1196–1197.
[25] S. Kishore, M. Maruthamuthu, Binding of rose Bengal onto bovine serum albumin, Proc. Indian Acad. Sci. (Chem. Sci.) 105 (1993) 279–285.
[26] S.M.T. Shaikh, J. Seetharamappa, P.B. Kandagal, D.H. Manjunatha, S. Ashoka, Spectroscopic investigations on the mechanism of interaction of bioactive dye with bovine serum albumin, Dyes Pigment. 74 (2007) 665–671.
[27] M.A.J. Rodgers, Picosecond fluorescence studies of rose-bengal in aqueous micellar dispersions, Chem. Phys. Lett. 78 (1981) 509–514.
[28] M. Mirenda, L.E. Dicelio, E. San Román, Effect of molecular interactions on the photophysics of Rose Bengal in polyelectrolyte solutions and self-assembled thin films, J. Phys. Chem. B 112 (2008) 12201–12207.
[29] M.J. Simpson, H. Poblete, M. Griffith, E.I. Alarcon, J.C. Scaiano, Impact of dye-protein interaction and silver nanoparticles on rose bengal photophysical behavior and protein photocrosslinking, Photochem. Photobiol. 89 (2013) 1433–1441.
[30] F. Tanaka, N. Mataga, Dynamic depolarization of interacting fluorophores. Effect of internal rotation and energy transfer, Biophys. J. 39 (1982) 129–140.
[31] V. Levi, F.L. Gonzalez Flecha, Reversible fast-dimerization of bovine serum albumin detected by fluorescence resonance energy transfer, Biochim. Biophys. Acta 1599 (2002) 141–148.
[32] M.I. Stefan, N. Le Novère, Cooperative binding, PLOS Comput. Biol. 9 (2013) 1–6.
[33] J.N. Weiss, The Hill equation revisited: uses and misuses, FASEB J. 11 (1997) 835–841.
[34] M.V. Encinas, E.A. Lissi, Evaluation of partition constants in compartmentalised systems from fluorescence quenching data, Chem. Phys. Lett. 91 (1982) 55–57.
[35] E. Alarcón, A. Aspée, E.B. Abuin, E.A. Lissi, Evaluation of solute binding to proteins and intra-protein distances from steady state fluorescence measurements, J. Photochem. Photobiol. B: Biol. 106 (2012) 1–17.
[36] L.E. Cramer, K.G. Spears, Hydrogen bond strengths from solvent-dependent lifetimes of Rose Bengal dye, J. Am. Chem. Soc. 100 (1978) 221–227.
[37] A. Srivastava, S. Doraiswamy, Rotational diffusion of rose bengal, J. Chem. Phys. 103 (1995) 6197–6205.
[38] J. Yguerabide, H.F. Epstein, L. Stryer, Segmental flexibility in antibody molecule, J. Mol. Biol. 51 (1970) 573–590.
[39] N. Mataga, H. Chosrowjan, Y. Shibata, F. Tanaka, Ultrafast fluorescence quenching dynamics of flavin chromophores in protein nanospace, J. Phys. Chem. B 102 (1998) 7081–7084.
[40] R.L. Jensen, J. Arnbjerg, H. Birkedal, P.R. Ogilby, Singlet oxygen's response to protein dynamics, J. Am. Chem. Soc. 133 (2011) 7166–7173.
[41] R.L. Jensen, J. Arnbjerg, P.R. Ogilby, Reaction of singlet oxygen with tryptophan in proteins: a pronounced effect of the local environment on the reaction rate, J. Am. Chem. Soc. 134 (2012) 9820–9826.
[42] A. Michaeli, J. Feitelson, Reactivity of singlet oxygen toward amino acids and peptides, Photochem. Photobiol. 59 (1994) 284–289.
[43] M.J. Davies, The oxidative environment and protein damage, BBA-Proteins Proteomics 1703 (2005) 93–109.
[44] D.I. Pattison, A.S. Rahmanto, M.J. Davies, Photo-oxidation of proteins, Photochem. Photobiol. Sci. 11 (2012) 38–53.
[45] P.R. Ogilby, Singlet oxygen: there is indeed something new under the sun, Chem. Soc. Rev. 39 (2010) 3181–3209.
[46] J. Baier, M. Maier, R. Engl, M. Landthaler, W. Bäumler, Time-resolved investigations of singlet oxygen luminescence in water, in phosphatidylcholine, and in aqueous suspensions of phosphatidylcholine or HT29 Cells, J. Phys. Chem. B 109 (2005) 3041–3046.